Journal of Marine Research, 62, 153–167, 2004

Journal of
MARINE RESEARCH

Volume 62, Number 2

Exchange processes and watermass modifications along the subarctic front in the North Pacific: Oxygen consumption rates and net carbon flux

by Murat Aydin[1,2], Zafer Top[1] and Donald B. Olson[1]

ABSTRACT

Exchange processes along the subarctic front and the modification of subpolar water in the North Pacific are investigated using tracer data from World Ocean Circulation Experiment P14N and P17N lines. The North Pacific Current transports water on both sides of the subarctic front from the western to eastern North Pacific. During this transport, subpolar water from the western subpolar gyre becomes warmer and saltier through the main thermocline via isopycnal mixing with subtropical water. It is shown that this modified subpolar water of western origin is the primary source of well-ventilated water to the eastern subpolar gyre. The isopycnal mixing along the subarctic front is quantified with a two end-member linear mixing analysis using potential temperature, which allowed estimates of oxygen consumption and nitrate remineralization on intermediate layers. Based on the oxygen consumption estimates and temporal information from transient tracers, the vertically integrated oxygen consumption rate is calculated to be 2.1 ± 0.4 M $m^{-2}y^{-1}$ in the 132–706 m depth range. This implies a net carbon flux of approximately 19 ± 4 gC $m^{-2}y^{-1}$ out of the euphotic zone.

1. Introduction

In the western North Pacific, watermass modification occurs near the energetic confluence region between two boundary currents the Oyashio and the Kuroshio. This "perturbed region (Kawai, 1972)" is generally accepted as the primary formation site of the North Pacific Intermediate Water (Yasuda *et al.,* 1996; Talley *et al.,* 1995; Talley, 1993) where surface water is dense enough to penetrate intermediate layers. The formation of the North

1. Rosenstiel School of Marine and Atmospheric Science, University of Miami, Miami, Florida, 33149, U.S.A.
2. Present address: University of California, Earth System Science, Irvine, California, 92697, U.S.A. ***email: maydin@uci.edu***

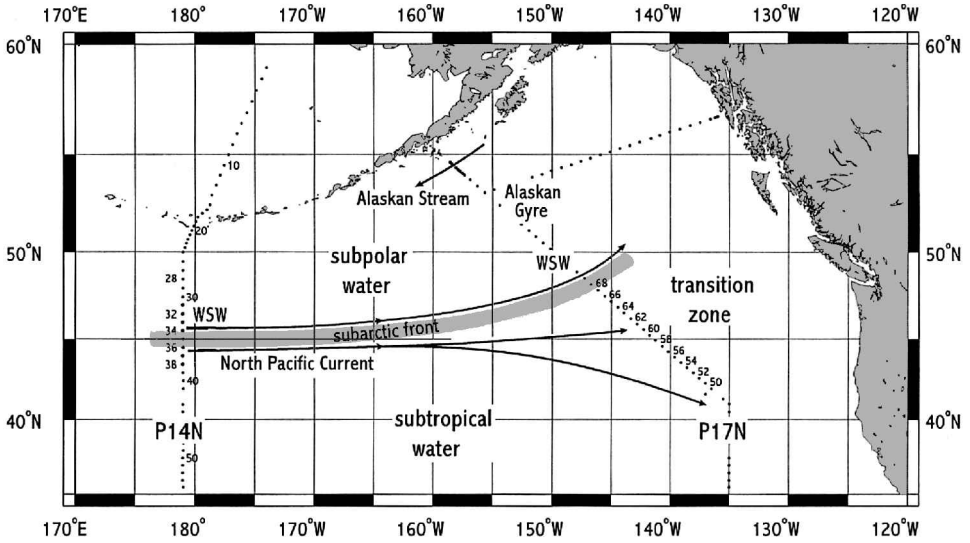

Figure 1. An illustration of the general circulation features and the distribution of different regions based on properties observed in WOCE P14N and P17N sections. The subpolar water in the eastern North Pacific is identified with a shallow, isothermal halocline that lies below the seasonal pycnocline. The sharp, isopycnal gradient of temperature and salinity observed between the subpolar and subtropical water is identified as the subarctic front. WSW lies in a narrow band on the subpolar side of the subarctic front and it is transported eastward as part of the North Pacific Current. The properties of the water in the transition zone are a mixture of subpolar and subtropical characteristics.

Pacific Intermediate Water is the primary ventilation process in the North Pacific as the low salinity and high oxygen signature of the subpolar surface water is dispersed into the subtropical gyre. Despite lacking the complicated boundary current dynamics and the associated high eddy kinetic energy, the eastern basin can also play a role in the watermass dynamics of the North Pacific, albeit a less significant one. The Alaskan Gyre is shown to be a modification site and cross-gyre exchange processes are likely to occur as the distribution of properties on either side of the gyre boundary indicate that exchange is essential to maintain the temperature and salinity structure observed in the central and the eastern North Pacific (You *et al.,* 2000; Aydin *et al.,* 1998; Musgrave *et al.,* 1992; Van Scoy *et al.,* 1991).

The Aleutian Islands act as a geographic boundary that can split the subpolar gyre and allow the Alaskan Gyre to form a closed circulation, leaving the North Pacific Current (NPC) as the only direct connection between the western and eastern basins. The NPC flows eastward along the subarctic front (Fig. 1), which is characterized by an abrupt change in temperature and salinity where the cold and fresh water of the subpolar gyre meets the warm and salty subtropical water to the south. The importance of the NPC as a

link between the west and the east was demonstrated with the identification of subpolar water from the west in the eastern subpolar North Pacific as the Western Subpolar Waters (WSW) (Aydin *et al.,* 1998).

In the following sections, first the WSW is identified along the northern edge of the subarctic front to show that it originates in the western subpolar gyre and is modified by the mixing of warmer and saltier subtropical water. The existence and the extent of this mixing are of particular importance since it has implications on the property distributions in the whole of the subpolar gyre. The pycnocline of the subpolar gyre in the North Pacific is characterized by a relatively salty and warm halocline which can only be maintained by an outside source of heat and salt. It has been suggested that the source of the heat and salt is a geostrophic inflow of subtropical water from the east of Japan into the Alaskan Gyre (Ueno and Yasuda, 2000). In this work, isopycnal mixing along the flow path of the North Pacific Current is proposed as an alternative mechanism that supplies heat and salt to the halocline of the subpolar gyre.

Following the quantification of the modification along the subarctic front with an isopycnal mixing analysis, the integrated oxygen consumption rate and the corresponding carbon flux out of the euphotic zone are calculated. The capacity of the world ocean to sequester carbon has gained importance with the recognition of the role of carbon dioxide (CO_2) on global climate as an atmospheric greenhouse gas. The new production in the euphotic zone, or the net carbon flux out of it, is a critical parameter in determining the carbon flux between the atmosphere and the world ocean. Spitzer and Jenkins (1989) estimated the new production in the subtropical Atlantic near Bermuda to be 36–60 gC $m^{-2}y^{-1}$, which was approximately an order of magnitude higher than the earlier estimates of Eppley and Peterson (1979) of 5–6 gC $m^{-2}y^{-1}$ for the transitional water between subpolar and subtropical zones. More recent estimates from the North Pacific Ocean appear to converge in between numbers with net carbon production estimates of 32 gC $m^{-2}y^{-1}$ for the subtropical North Pacific (Emerson *et al.,* 1997, 2001) and 24 gC $m^{-2}y^{-1}$ for Station P in the subpolar North Pacific (Emerson *et al.,* 1991, 2001; Boyd and Harrison, 1999; Varela and Harrison, 1999). Here the net carbon flux out of the euphotic zone is inferred from the properties of the underlying intermediate layer water and the findings are in agreement with the recent estimates that are based on observations in the surface layers.

The results are based primarily on linear mixing equations, which are solved for potential temperature (θ) and salinity profiles that represent subtropical and subpolar end-members of the mixing process. The time scale of the mixing process is estimated with the temporal information provided by transient tracer techniques like tritium-helium (^{3}H-^{3}He) dating (Clarke *et al.,* 1976; Jenkins *et al.,* 1983) and chlorofluorocarbon (CFC) dating (Fine *et al.,* 1988; Doney and Bullister, 1992). All data are from P14N and P17N lines of the World Ocean Circulation Experiment (WOCE) (Fig. 1). Both P14N and P17N sections of WOCE were completed in the summer of 1993 and the current work does not address possible effects of temporal variability observed in the region (Trenberth and Hurrell, 1994; Lagerloef, 1995).

2. WSW in the North Pacific

In the WOCE P17N data from the eastern North Pacific, the WSW is identified to the south of the Alaskan Gyre between 48–52N in the eastward flow regime of the North Pacific Current with unique properties in θ, salinity, oxygen, nutrients, and CFCs (Aydin *et al.,* 1998). Although it displays the characteristic features of the summer time subpolar North Pacific with a thermally stratified seasonal pycnocline overlying a strong halocline, the WSW is distinguished from the Alaskan Gyre with more heat and salt through the halocline ($\sigma_\theta < 26.7$) (Fig. 2a), and higher oxygen through 27.5 σ_θ (Fig. 2b). It is unlikely that local processes in the eastern North Pacific can account for such tracer distributions because winter ventilation processes are expected to peak at the center of the Alaskan Gyre where water is not as well ventilated compared with the WSW despite being colder on $\sigma_\theta < 26.7$ (Fig. 2a, b). It is also considered that water from the Alaskan Stream, which is warmer and saltier than the Alaskan Gyre, can recirculate around and modify the water that lies to the south of the Alaskan Gyre to be warmer and saltier. However, the Alaskan Stream is poorly ventilated with low oxygen and CFC concentrations (Aydin *et al.,* 1998) and it is unlikely to be a significant source to the well-ventilated WSW. It is, therefore, suggested that the WSW is transported into the region from the west via the NPC, acquiring heat and salinity from the subtropical gyre along its advective path (Fig. 1). WOCE P14N data are analyzed to investigate whether the end-members that make up the WSW can be isolated upstream in the central North Pacific.

In the central North Pacific, the subarctic front between the subtropical and subpolar gyres is observed near 45N at Station 35 in the P14N section (Fig. 3a). There is a secondary front near Station 40 in the subtropical gyre, and only to the south of this second front is the North Pacific Intermediate Water evident as a salinity minimum centered around 26.8 σ_θ (Fig. 3b). On the subpolar side of the subarctic front, the temperature minimum that lies below the seasonal pycnocline does not extend to 45N and covers only a part of the subpolar region (Fig. 3a). The anamolous water identified by Stations 32–34 in the subpolar gyre and 36–40 in the subtropical gyre is in the core of the eastward flow of the NPC (Fig. 4a) and is better oxygenated than the rest of the subpolar and subtropical water that lies to the north and south, respectively (Fig. 4b). It is suggested that the well-ventilated subpolar water identified by Stations 32–34 represents the WSW in P14N, and during the eastward transport, its properties are modified via isopycnal mixing with subtropical water identified by Stations 36–40. The effects of this mixing are evident as the WSW is warmer in P17N than it is in P14N through the halocline and the main thermocline (Fig. 5a) but the seasonal pycnocline in P17N is fresher, colder, and shallower due to surface fluxes. The oxygen concentrations decrease downstream as expected with the largest change on $\sigma_\theta < 26.9$ (Fig. 5b).

The properties of the WSW in P17N are analyzed, considering linear mixing between the two end-members. Isopycnal mixing on a given density layer is represented with Eq. (1), in which X and C denote the mixing fraction and the concentration of a property, respectively. Eq. (2) implies that the mixing fractions add up to unity. Eqs. (1) and (2) are

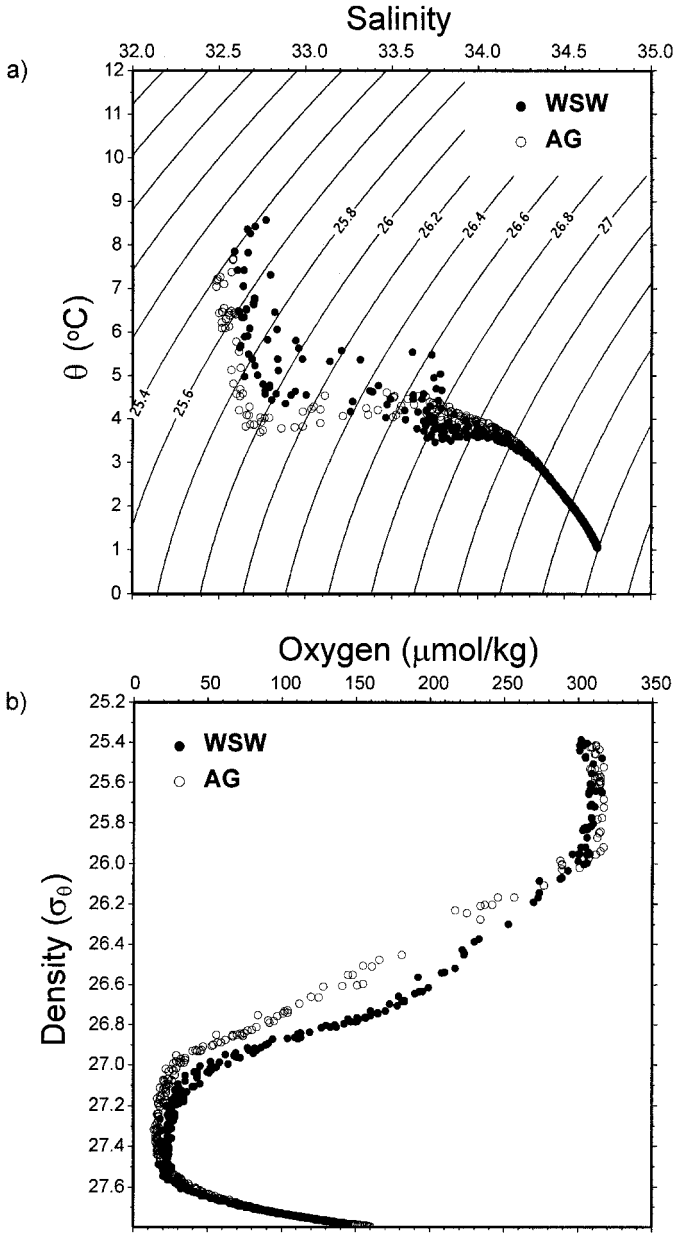

Figure 2. (a) The WSW is colder and fresher than the Alaskan Gyre water (AG) on intermediate isopycnals down to 27.2 σ_θ but warmer and saltier in the overlying halocline and the seasonal pycnocline, indicating a subtropical input to these layers. (b) The oxygen content of WSW is higher than the AG through the water column, distinguishing the WSW as the better ventilated subpolar water, which originates in the western basin of the subpolar North Pacific.

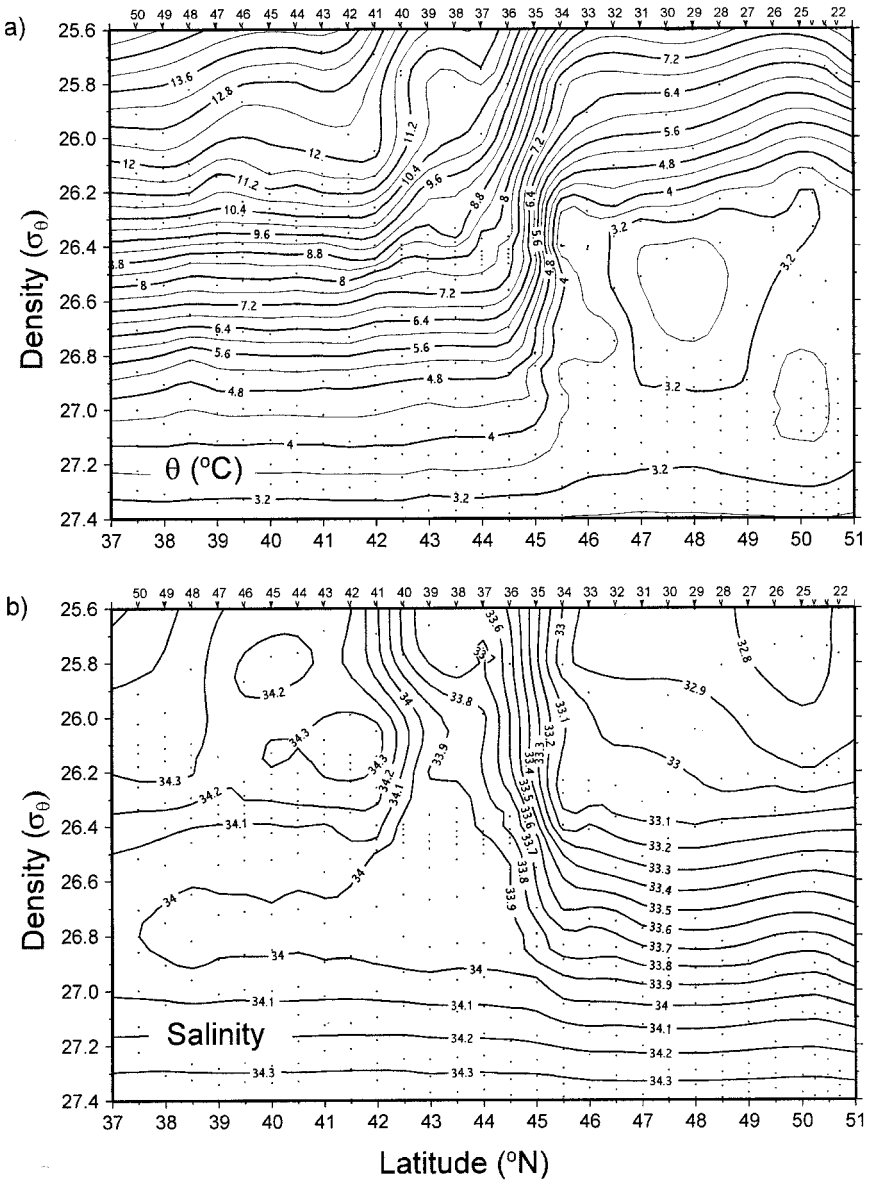

Figure 3. (a) P14N potential temperature (θ) section. The subarctic front that separates subpolar and subtropical gyres is observed at 45N. The stations 32–34 in the subpolar gyre differ from the other subpolar stations as the minimum does not extend all the way to the boundary. Similarly, Stations 36–40 differ from the subtropical stations to the south as shallower layers are considerably cooler. (b) P14N salinity section. Stations 36–40 are fresher on densities lighter than 26.5 σ_θ and they do not exhibit an intermediate salinity minimum that is the characteristic watermass of the subtropical gyre: the North Pacific Intermediate Water.

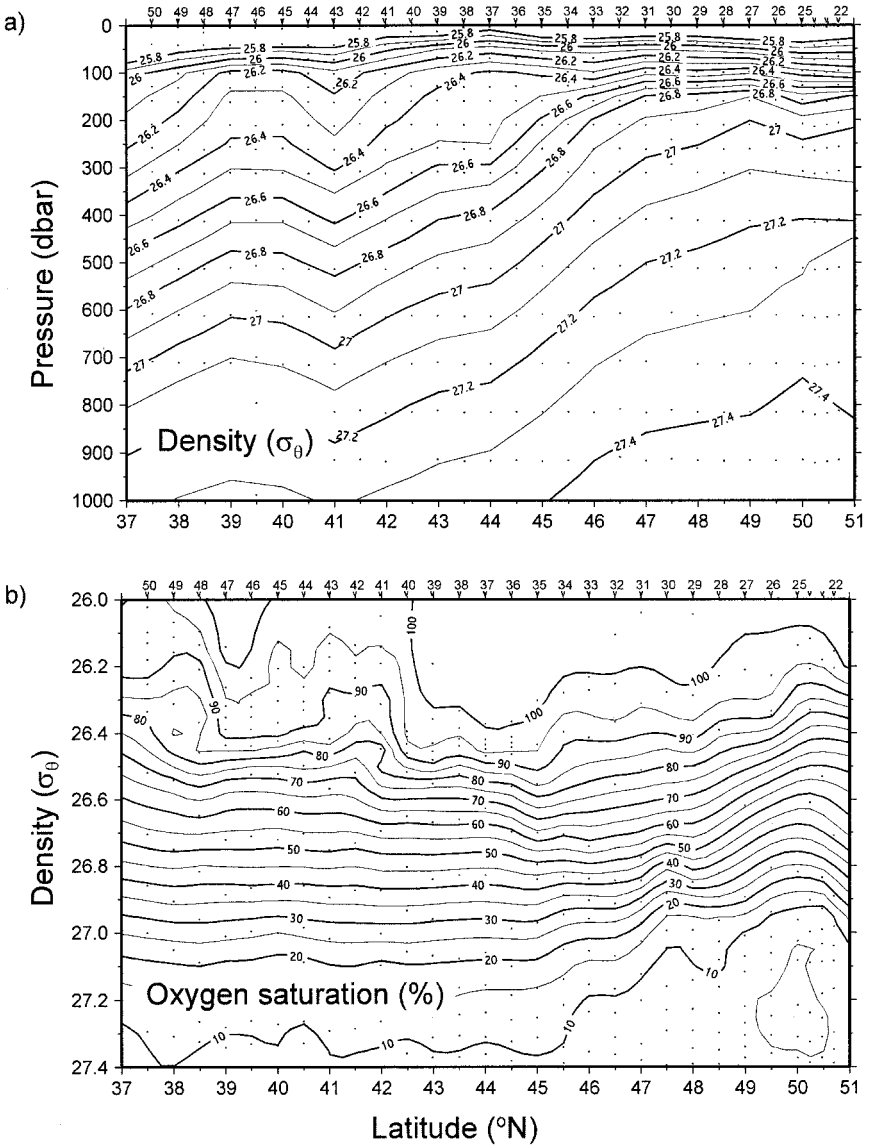

Figure 4. (a) P14N density section. The eastward flow of the North Pacific Current is evident between 42N and 47N. (b) P14N oxygen saturation section. The station groups 32–34 in the subpolar gyre and 36–40 in the subtropical gyre are better oxygenated than the rest of the stations in the respective gyres.

solved for θ and salinity, yielding the same mixing fractions within the uncertainties (Table 1). Subtropical water appears to contribute more to the shallower layers and the uncertainty in the calculated mixing fractions increase below 27.0 σ_θ. The uncertainties reported for the

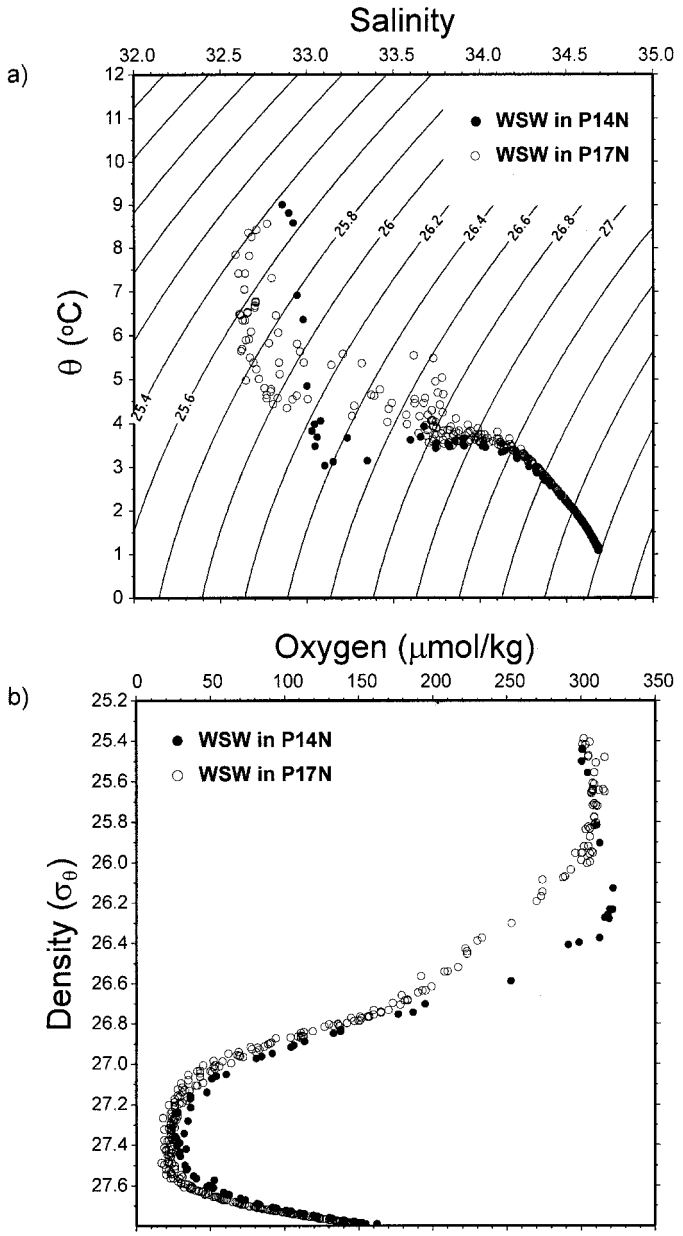

Figure 5. (a) The WSW is warmer and saltier in P17N than P14N through much of the water column except in the seasonal pycnocline, which reflects the effects of buoyancy fluxes at the ocean-atmosphere interphase. (b) The oxygen concentration in the WSW decreases as it is transported from the central to the eastern North Pacific.

Table 1. Average properties of end-members on density layers and the calculated mixing fractions.

Density	P14N Stns 32–34		P14N Stns 36–40		P17N WSW		X_{WSW}^{P14N}	
σ_θ	θ (°C)	Salinity	θ (°C)	Salinity	θ (°C)	Salinity	θ (°C)	Salinity
26.5	3.34 ± 0.57	33.30 ± 0.09	7.57 ± 0.11	33.93 ± 0.02	4.68 ± 0.51	33.47 ± 0.07	0.68 ± 0.15	0.72 ± 0.16
26.6	3.61 ± 0.47	33.45 ± 0.08	6.95 ± 0.14	33.95 ± 0.02	4.60 ± 0.47	33.59 ± 0.07	0.71 ± 0.18	0.73 ± 0.18
26.7	3.80 ± 0.25	33.60 ± 0.03	6.10 ± 0.09	33.94 ± 0.01	4.35 ± 0.38	33.68 ± 0.05	0.76 ± 0.19	0.78 ± 0.18
26.8	3.59 ± 0.06	33.71 ± 0.01	5.33 ± 0.07	33.94 ± 0.01	3.90 ± 0.24	33.75 ± 0.03	0.82 ± 0.15	0.85 ± 0.15
26.9	3.54 ± 0.06	33.83 ± 0.01	4.74 ± 0.05	33.98 ± 0.01	3.73 ± 0.17	33.85 ± 0.02	0.84 ± 0.16	0.86 ± 0.16
27.0	3.54 ± 0.09	33.95 ± 0.01	4.34 ± 0.06	34.05 ± 0.01	3.70 ± 0.09	33.97 ± 0.01	0.80 ± 0.17	0.82 ± 0.20
27.1	3.48 ± 0.07	34.07 ± 0.01	4.04 ± 0.06	34.14 ± 0.01	3.63 ± 0.07	34.09 ± 0.01	0.73 ± 0.20	0.73 ± 0.23
27.2	3.34 ± 0.06	34.18 ± 0.01	3.70 ± 0.04	34.22 ± 0.01	3.44 ± 0.05	34.19 ± 0.01	0.73 ± 0.23	0.77 ± 0.32

end-members in Table 1 reflect a $\pm 1\sigma$ confidence interval calculated as standard deviation of the mean, which are propogated through the mixing calculation to estimate the uncertainties in the calculated mixing fractions. The analysis is confined to density layers below 26.5 σ_θ to eliminate the effects of surface fluxes and to above 27.2 σ_θ, below which uncertainties increase rapidly due to diminishing θ and salinity gradients.

$$X_{WSW}^{P14N} \cdot C_{WSW}^{P14N} + X_{subtropic}^{P14N} \cdot C_{subtropic}^{P14N} = C_{WSW}^{P17N} \quad (1)$$

$$X_{WSW}^{P14N} + X_{subtropic}^{P14N} = 1 \quad (2)$$

3. Oxygen consumption along the subarctic front

The mixing fractions derived from θ are used to calculate the average oxygen concentration in WSW and compared with observations from P17N to estimate oxygen consumption during the transport of water from P17N to P14N (Fig. 6a). The difference between the estimates and the observations is a measure of the net biological oxygen consumption. Nitrate remineralization is estimated implementing the same calculation, using the average nitrate concentrations of the P14N end-members and of the WSW in P17N (Fig. 6b). Nitrate remineralization can also be estimated based on the calculated oxygen consumption numbers. On subsurface layers of the ocean, oxygen consumption is balanced by an equivalent nutrient remineralization with a Redfield N:$-O_2$ ratio of 16:172 (Takahashi *et al.,* 1985). The result of this Redfield consideration compares well to the nitrate remineralization estimates calculated with the mixing fractions (Fig. 6b), supporting the mixing fractions calculated from θ and salinity.

If the oxygen consumption estimates are evaluated considering the layer thicknesses and the time scale of the transport between P17N and P14N, oxygen consumption rates can be calculated as a flux (Table 2). The time scale estimates in this calculation are primarily based on ^{3}H-^{3}He and *p*CFC ages from the North Pacific. The WSW stations in P14N had not been sampled for ^{3}H-^{3}He; however, these data are available in Station 35 on $\sigma_\theta > 26.9$. Because the θ and salinity structure of Station 35 closely resembles the subtropical P14N stations and the subtropical component from P14N has a minor contribution to the WSW in P17N, a straightforward comparison of ^{3}H-^{3}He ages from Station 35 in P14N to WSW in P17N is not appropriate. Instead, age data from Station 35 are compared with age data from five P17N stations (50, 54, 57, 60, 64) (Fig. 7). These stations are in a similar latitude range as Stations 36–40 from P14N and are more heavily influenced by subtropical water (Fig. 1). The calculated age differences between P14N and P17N on 27.0, 27.1, and 27.2 σ_θ are 4, 6, and 9 years, respectively. Similar horizontal time scales can be discerned from *p*CFC-11 and *p*CFC-12 ages as 6 and 8 years on 27.2 σ_θ, respectively (Figs. 6e and 7b in Warner *et al.,* 1996). On a shallower isopycnal (26.8 σ_θ) the *p*CFC-11 and *p*CFC-12 time scales are 3 to 5 years (Figures 6d and 7a in Warner *et al.,* 1996). Maps of *p*CFC age based on a larger data set that includes WOCE sections indicate a constant spreading time of 4–5 years on 26.4, 26.8, and 27.2 σ_θ (Bullister *et al.,* submitted for review, 2004; ftp://ftp.pmel.noaa.gov/

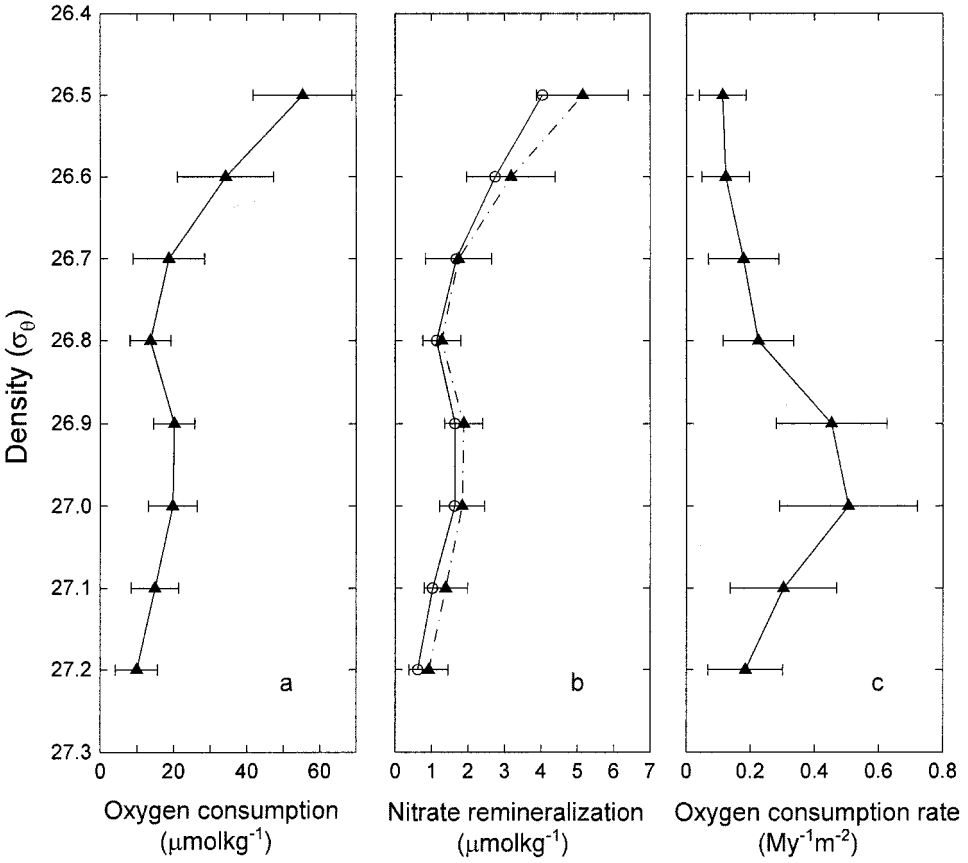

Figure 6. (a) Oxygen consumption profile calculated with mixing ratios. (b) Nitrate reminaralization calculated from mixing ratios (open circles-solid line) and nitrate remineralization calculated from the oxygen consumption profile (Fig. 6a) using a Redfield ratio (triangles-solid line). (c) Oxygen consumption rate calculated as a flux. The maximum in the oxygen consumption rate around 26.9 and 27.0 σ_θ is just near the top of the oxygen minimum zone observed in the main thermocline.

wocecfc/freon/pacific/pac_isopyc_maps). It is estimated that on layers shallower than 27.0 σ_θ, the transport between P14N and P17N takes about four years; on 27.1 and 27.2 σ_θ, we estimate that the time scale increases to 6 and 8 years based on the ^{3}H-^{3}He ages (Table 2). The resulting oxygen consumption rates (Fig. 6c) are low on shallow layers but increase to a subsurface maximum at 27.0 σ_θ, which lie just above the oxygen minimum zone in the main thermocline. These rates yield a depth integrated oxygen consumption rate of 2.1 $\pm$ 0.4 M m^{-2}y^{-1} in 26.5 and 27.2 σ_θ range that lie between 132–706 m (Table 2). The layer thicknesses and the transport time scales presented in Table 2 can also be used to quantify the heat transferred to the subpolar gyre. The mixing of warm water into the WSW between P14N and P17N transects is 5.3 $\pm$ 1.6 $\times$ 10^8 J m^{-2}, which corresponds to a heat flux of

Table 2. Oxygen consumption and oxygen consumption rate estimates on intermediate isopycnals.

σ_θ	Thickness (m)	Oxygen (μmol kg^{-1}) Estimated	Observed	Oxygen consumption (μmol kg^{-1})	Time (y)	Oxygen consumption rate (M m^{-2}y^{-1})
26.5	8.0 ± 4.3	270.3 ± 12.6	215.0 ± 4.9	55.3 ± 13.5	4 ± 1	0.11 ± 0.07
26.6	14.0 ± 5.5	231.7 ± 12.0	197.5 ± 5.2	34.2 ± 13.1	4 ± 1	0.12 ± 0.07
26.7	37.2 ± 7.3	194.3 ± 8.7	175.6 ± 4.5	18.7 ± 9.8	4 ± 1	0.18 ± 0.11
26.8	63.9 ± 5.2	152.0 ± 4.1	138.2 ± 3.9	13.8 ± 5.6	4 ± 1	0.23 ± 0.11
26.9	87.4 ± 6.2	109.7 ± 2.2	89.5 ± 5.2	20.2 ± 5.6	4 ± 1	0.45 ± 0.17
27.0	99.8 ± 7.2	74.0 ± 3.8	54.2 ± 5.4	19.8 ± 6.6	4 ± 1	0.51 ± 0.21
27.1	118.7 ± 6.6	51.4 ± 4.4	36.5 ± 4.7	14.9 ± 6.4	6 ± 2	0.30 ± 0.17
27.2	145.1 ± 5.0	37.0 ± 5.0	27.1 ± 2.9	9.9 ± 5.8	8 ± 2	0.18 ± 0.12
Total						**2.1 ± 0.4**

3.8 ± 1.2 W m^{-2}. In comparison, the net annual heat flux at the air-sea interface over the eastern subpolar North Pacific is approximately an order of magnitude larger (Josey *et al.,* 1999).

The effects of seasonal changes like the mixed layer deepening and shoaling of isopycnals are not considered in these calculations and both P14N and P17N data are summer time observations. The mixed layer reaches depths over a 100 m at a density of 26.4 to 26.5 σ_θ near dateline in the subpolar gyre (Levitus *et al.,* 1994; Levitus and Boyer, 1994), suggesting the upper most part of the water column selected for the current

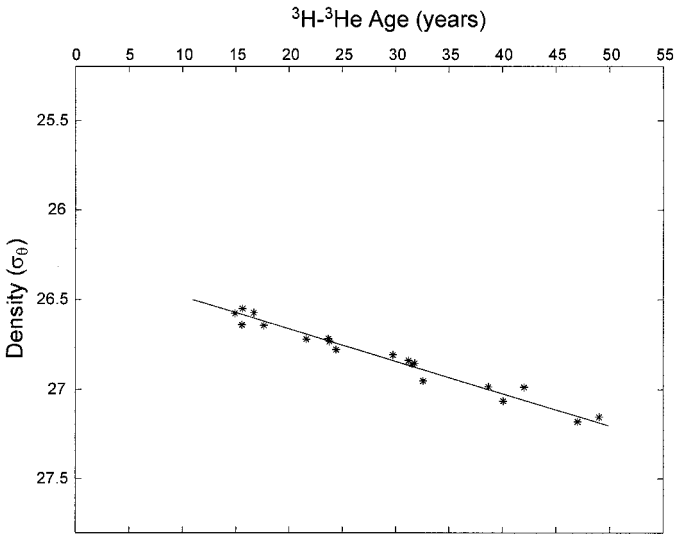

Figure 7. Linear fit to the ^{3}H-^{3}He age data from the transition zone in P17N is used to depict ages for 27.0, 27.1, and 27.2 σ_θ.

calculations may be influenced by processes that occur in the euphotic zone during the coldest periods of the year. However, the oxygen consumption rate peaks around 27.0 σ_θ and the cumulative contribution from 26.5 and 26.6 σ_θ is only 10% of the total, diminishing the significance of any additional uncertainty that may apply to these shallower isopycnals.

The oxygen consumption rate of 2.1 $\pm$ 0.4 M $m^{-2}y^{-1}$ implies a carbon flux of approximately 19 $\pm$ 4 gC $m^{-2}y^{-1}$. The actual carbon flux out of the euphotic zone must be somewhat larger since the oxygen consumption below 700 m is ignored in this calculation. Lutz *et al.* (2002) show that flux of particulate organic carbon is subject to high regional variability in the world ocean and estimate the fraction of carbon flux that reaches depths greater than 1500 m to vary between 0.3 to 30% (5.7% global average) of the export out of the euphotic zone. The current estimate is in good agreement with net carbon production estimates of 32 gC $m^{-2}y^{-1}$ for subtropical North Pacific (Emerson *et al.,* 1997, 2001) and 24 gC $m^{-2}y^{-1}$ for Station P in the subpolar North Pacific (Emerson *et al.,* 1991, 2001; Boyd and Harrison, 1999; Varela and Harrison, 1999). However, the agreement does not extend to results from remote sensing methods as the maps of mean annual export production of Falkowski *et al.* (1998) based on satellite ocean color measurements show the net production in the North Pacific near the subtropical-subpolar gyre boundary to be 2–3 times the present estimate at 50–75 gC $m^{-2}y^{-1}$.

4. Conclusions

The tracer data from WOCE P14N and P17N are used in a linear isopycnal mixing analysis to show that horizontal mixing along the frontal zone between subpolar and subtropical gyres is substantial and shifts the buoyancy budget in the WSW to a warmer and saltier regime on intermediate layers. It is evident that this exchange has an overall impact on the properties of the eastern subpolar gyre. Considering how the properties of the Alaskan Gyre and Alaskan Current systems are interlinked (Aydin *et al.,* 1998), the extra heat and salt observed in the eastern subpolar gyre appears to be a direct result of this exchange process. The heat flux into the subpolar gyre as a result of this exchange is calculated to be 3.8 $\pm$ 1.2 W m^{-2}. If there is a feedback mechanism in the subpolar system such that the western subpolar gyre is influenced by what happens in the east through complex mixing mechanisms that involves the Bering Sea, this warm and salty signature is likely to weaken and erode to deeper layers during the process.

It is shown that the North Pacific Current is an advective path for the well-ventilated water formed in the western subpolar gyre. The current analysis provides further evidence that the best ventilated intermediate water found around the Alaskan Gyre is transported into the region from the west. It is, therefore, unlikely that processes in the eastern subpolar gyre play a role in the ventilation of intermediate layers in the North Pacific through formation of the North Pacific Intermediate Water. Instead, the evidence points to the western subpolar gyre as a common source of well-ventilated water to the subtropical as well as the eastern subpolar gyres.

The current mixing analysis yields an integrated oxygen consumption rate of 2.1 ± 0.4 M $m^{-2}y^{1}$ in 132–706 m depth range along the subarctic front. This requires a net carbon flux of approximately 19 ± 4 gC $m^{-2}y^{-1}$ out of the euphotic zone to support the oxygen consumption in the top 600 m of the thermocline in the subpolar North Pacific. The total carbon export out of the euphotic zone should be larger since the current calculations do not account for the oxygen consumption below 700 m. It is not possible to assess whether and how much these results would vary with the variability of climatological conditions in the North Pacific without additional data sets. However, since the results are based on oceanographic tracer data, they should not be regarded as a snap shot but rather an observation of average conditions in the North Pacific over a period of time.

Acknowledgments. We would like to thank William B. Johns, Rana A. Fine, Göte H. Östlund and Ellen R. M. Druffel for their input. We would also like to thank the chief scientists of WOCE P14N and P17N sections, Gunnar I. Roden and David L. Musgrave, for the hydrographic, oxygen, and nutrient data. This work was supported by the National Science Foundation through grant OCE 92-16995.

REFERENCES

Aydin, M., Z. Top, R. A. Fine and D. B. Olson. 1998. Modification of the intermediate waters in the northeastern subpolar Pacific. J. Geophys. Res., *103,* 30923–30940.

Boyd, P. and P. J. Harrison. 1999. Phytoplankton dynamics in the NE subarctic Pacific. Deep-Sea Res. II, *46,* 2405–2432.

Clarke, W. B., W. J. Jenkins and Z. Top. 1976. Determination of tritium by mass spectrometric measurements of ^{3}He. Inter. J. Appl. Radiation Isotopes, *27,* 515–522.

Doney, S. C. and J. L. Bullister. 1992. A chlorofluorocarbon section in the eastern North Atlantic. Deep-Sea Res., *39,* 1857–1883.

Emerson, S., S. Mecking and J. Abell. 2001. The biological pump in the subtropical North Pacific Ocean: Nutrient sources, Redfield ratios, and recent changes. Global Biogeochem. Cycles, *15,* 535–554.

Emerson, S., P. D. Quay, D. Karl, C. Winn, L. Tupas and M. Landry. 1997. Experimental determination of the organic carbon flux from open-ocean surface waters. Nature, *389,* 951–954.

Emerson, S., P. D. Quay, C. Stump, D. Wilbur and M. Knox. 1991. O_2, Ar, N_2, and ^{222}Rn in surface waters of the subarctic ocean: Net biological O_2 production. Global Biogeochem. Cycles, *5,* 49–69.

Eppley, R. W. and B. J. Peterson. 1979. Particulate organic matter flux and planktonic new production in the deep ocean. Nature *282,* 677–680.

Falkowski, P. G., R. T. Barber and V. Smetacek. 1998. Biogeochemical controls and feedbacks on ocean primary production. Science, *281,* 200–206.

Fine, R. A., M. J. Warner and R. F. Weiss. 1988. Water mass modification at the Agulhas retroflection: chlorofluoromethane studies. Deep-Sea Res., *35,* 311–332.

Jenkins, W. J., D. E. Lott, M. W. Pratt and R. D. Boudrea. 1983. Anthropogenic tritium in South Atlantic bottom water. Nature, *305,* 45–46.

Josey, S., E. Kent and P. Taylor. 1999. New insights into the ocean heat budget closure problem from analysis of the SOC air-sea flux climatology. J. Climate, *12,* 2856–2880.

Kawai, H. 1972. Hydrography of Kuroshio Extention. Kuroshio: Physical Aspects of the Japan Current, H. Stommel and K. Yoshida, eds., University of Washington Press, 235–352.

Lagerloef, G. S. E. 1995. Interdecadal variations in the Alaskan Gyre. J. Phys. Oceanogr., *25,* 2242–2258.

Levitus, S. and T. P. Boyer. 1994. World Ocean Atlas 1994, Vol. 4, Temperature. NOAA Atlas NESDIS 4, U.S. Government printing office, Washington, DC, 117 pp.

Levitus, S., R. Burgett and T. P. Boyer. 1994. World Ocean Atlas 1994, Vol. 3, Salinity. NOAA Atlas NESDIS 3, U.S. Government printing office, Washington, DC, 99 pp.

Lutz, M., R. Dunbar and K. Caldeira. 2002. Regional variability in the vertical flux of particulate organic carbon in the ocean interior. Global Biogeochem. Cycl., *16,* 10.1029/2000GB001383.

Musgrave, D. L., T. J. Weigartner and T. C. Royer. 1992. Circulation and hydrography in the northwestern Gulf of Alaska. Deep-Sea Res., *39,* 1499–1519.

Spitzer, W. S. and W. J. Jenkins. 1989. Rates of vertical mixing, gas exchange, and new production: Estimates from seasonal gas cycles in the upper ocean near Bermuda. J. Mar. Res., *47,* 169–196.

Takahashi, T., W. S. Broecker and S. Langer. 1985. Redfield ratio based on chemical data from isopycnal surfaces. J. Geophys. Res., *90,* 6907–6924.

Talley, L. D. 1993. Distribution and formation of North Pacific Intermediate Water. J. Phys. Oceanogr., *23,* 517–537.

Talley, L. D., Y. Nagata, M. Fujimura, T. Iwao, T. Kono, D. Inagake, M. Hirai and K. Okuda. 1995. North Pacific Intermediate Water in the Kuroshio/Oyashio mixed water region. J. Phys. Oceanogr., *25,* 475–501.

Trenberth, K. E. and J. W. Hurrell. 1994. Decadal atmosphere-ocean variations in the Pacific. Climate Dyn., *9,* 303–319.

Ueno, H. and I. Yasuda. 2000. Distribution and formation of the mesothermal structure (temperature inversions) in the North Pacific subarctic region. J. Geophys. Res., *105,* 16885–16897.

Van Scoy, K. A., R. A. Fine and H. G. Östlund. 1991. Two decades of mixing tritium into the North Pacific Ocean. Deep-Sea Res., *38,* (Suppl. 1), 191–219.

Varela, D. E. and P. J. Harrison. 1999. Seasonal variability in nitrogenous nutrition of phytoplankton assemblages in the northeastern subarctic Pacific Ocean. Deep-Sea Res. II, *46,* 2505–2538.

Warner, M. J., J. L. Bullister, D. P. Wisegarver, R. H. Gammon and R. F. Weiss. 1996. Basin-wide distributions of chlorofluorocarbons CFC-11 and CFC-12 in the North Pacific: 1985–1989. J. Geophys. Res., *101,* 20525–20542.

Yasuda, I., K. Okuda and Y. Shimizu. 1996. Distribution and modification of North Pacific Intermediate Water in the Kuroshio-Oyashio interfrontal zone. J. Phys. Oceanogr., *26,* 448–465.

You, Y. Z., N. Suginohara, M. Fukasawa, I. Yasuda, I. Kaneko, H. Yoritaka and M. Kawamiya. 2000. Roles of the Okhotsk Sea and Gulf of Alaska in forming the North Pacific Intermediate Water. J. Geophys. Res., *105,* 3253–3280.

Received: *3 April, 2002;* revised: *10 February, 2004.*